Bandwidth Compressed Waveform for 60 GHz Millimeter-Wave Radio over Fiber Experiment

Tongyang Xu, *Student Member, IEEE*, Spiros Mikroulis, *Member, IEEE*, John E. Mitchell, *Senior Member, IEEE*, and Izzat Darwazeh, *Senior Member, IEEE*

Abstract—**A bandwidth compressed waveform termed spectrally efficient frequency division multiplexing (SEFDM) is experimentally demonstrated in a 60 GHz millimeter-wave (mm-wave) radio-over-fiber (RoF) scenario to increase transmission data rates without changing signal bandwidth and modulation format. Experimental results show the advantages of SEFDM and confirm that the bit rate of SEFDM signals can be substantially higher than that of OFDM signals. Experimentally, a 2.25 Gbit/s 4QAM OFDM signal is transmitted through 250 meters of OM-1 multi-mode fiber (MMF) and then it is optically up converted to 60 GHz band at the photodiode before delivery to a millimeter wave antenna for transmission over a 3 meter wireless link. The work demonstrates that when the OFDM signal is replaced by an SEFDM signal using the same modulation format and occupying the same bandwidth, the bit rate can be increased, by a factor of up to 67%, to 3.75 Gbit/s at the expense of a 3 dB power penalty. Additionally, a bandwidth compressed 4QAM SEFDM is shown to outperform an 8QAM OFDM of the same spectral efficiency, thereby verifying that a lower order modulation format may replace a higher order one and achieve performance gain.**

Index Terms—**Radio over fiber, 5G, fiber wireless, millimeter wave, spectral efficiency, OFDM, SEFDM, non-orthogonal.**

I. Introduction

SPECTRUM is a scarce and expensive resource. The exponential growth in demand for broadband services is leading to increased research in new modulation formats and system architectures aiming to utilize the available, yet limited, spectrum. In the current standarized 4th generation (4G) wireless network [1], up to 100 MHz channel bandwidth is allocated to meet high data rate requirements using carrier aggregation techniques. Due to the limited available bandwidth in the low GHz frequencies, the current standards are unable to support higher data rates. The increasing demand of high speed data rates may be addressed by the utilization of millimeter-wave (mm-wave) [2] radio frequencies, which have wider unlicensed signal bandwidths. The propagation characteristics at mm-wave frequencies limit their application to short distance wireless communication scenarios. In order to maintain the wide band benefit at mm-wave frequencies and extend the coverage, a hybrid radio over fiber (RoF) technique [3] is introduced as an alternative solution. Such a hybrid system has several advantages over typical fiber and wireless systems

alone since it merges both optical and wireless benefits. On the one hand, the fiber link provides low attenuation to mm-wave signals and the supported transmission distance can be significantly increased. On the other hand, the wireless link provides the flexibility of ubiquitous networking.

Future 5th generation (5G) wireless networks [4] should provide higher data rates within a limited bandwidth. One way is to use multicarrier transmission schemes. Commonly, orthogonal frequency division multiplexing (OFDM) [5] signals are used in mm-wave RoF systems [6][7][8]. One reason is OFDM's high spectral efficiency using orthogonally overlapping sub-carriers. Another reason is that OFDM can simultaneously mitigate dispersion effects from fiber links and multipath fading effects from wireless links. Due to the orthogonality property of OFDM signals, signal generation and channel compensation are relatively simple. However, in a practical transmission scenario, distortions either from wireless or optical fiber links could degrade the orthogonality between OFDM sub-carriers. In such cases, additional compensation algorithms are required at the receiver. Considering the expected distortions, a technique termed SEFDM was originally proposed in [9] where sub-carriers are intentionally arranged to be non-orthogonal. Thus, the orthogonality requirement is relaxed and both the spectral efficiency and associated channel capacity [10] are improved, at the expense of added receiver complexity [11]. This technique has been experimentally implemented in wireless [12], optical [13][14], and RoF [15][16] systems, where experimental validation showed that not only bandwidth is saved in SEFDM when compared to an equivalent OFDM system with the same modulation cardinality, but also when comparing SEFDM to an OFDM system with the same spectral efficiency, better error performance is obtained. There are other similar techniques that have been proposed for the purpose of improving spectral efficiency. Faster than Nyquist (FTN) [17] is a time-domain non-orthogonal technique, which transmits data at a rate beyond the Nyquist limit. Furthermore, a mixed domain technique termed time frequency packing (TFP), was proposed in [18] and which, if applied in a multicarrier scenario, may be viewed as a combination of SEFDM and FTN. TFP was demonstrated recently in a coherent optical system [19], showing advantages over standard non-spectrally efficient methods. Optical systems have used a related spectrally efficient technique termed fast orthogonal frequency division multiplexing (FOFDM), where one dimentional modulation schemes can be used. FOFDM was initially proposed for wireless systems in [20], adapted to optical systems in [21], investigated (through

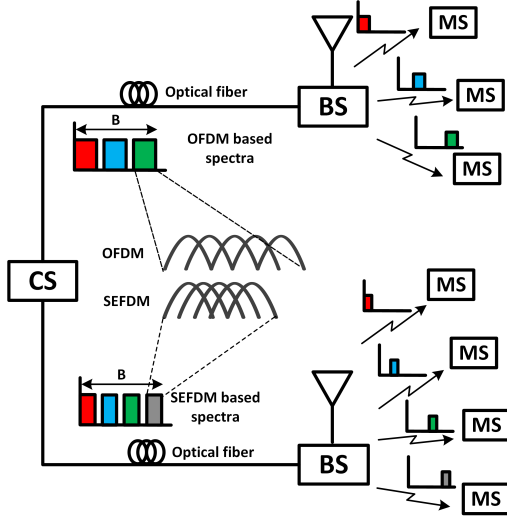simulations) for 60 GHz RoF implementation in [22] and recently demonstrated in an optical system in [23].

Figure 1. Application scenario of SEFDM in fiber wireless networks where CS indicates central station, BS indicates base station and MS indicates mobile station. Both OFDM and SEFDM sub-carrier packing schemes for each band are illustrated.

In this work, we consider advantages of both mm-wave and SEFDM. Recalling that in the mm-wave frequencies range, there exists a wide unlicensed bandwidth while SEFDM is a bandwidth compression technique, the combination of the two allows a higher number of aggregated sub-carriers in a given bandwidth. This can result in a scenario, shown in Fig. 1, where more users (more signal bands) can share the same overall bandwidth. For each signal band, either in the OFDM or SEFDM scenarios, the same number of sub-carriers are aggregated. It is evident that the bandwidth of each band in the SEFDM scenario is narrower than that of the OFDM scenario. In order to simplify the demonstration, one mobile station (MS) is assumed to occupy the entire bandwidth in this experimental work. In an integrated multimode fiber (250 meters) and wireless (60 GHz over 3 meters) link, this work demonstrates that the OFDM system achieves 2.25 Gbit/s while a bandwidth equivalent SEFDM can reach up to 3.75 Gbit/s.

The rest of the paper is organized as follows. Section II gives a description of the SEFDM system principle especially the crucial digital signal processing including signal generation, channel compensation and signal detection. Section III describes the experimental setup for the mm-wave SEFDM transceiver with an integrated mm-wave wireless and fiber links and Section IV shows the measured results from the experimental testbed. Finally, Section V concludes the paper.

II. Digital Signal Processing of SEFDM

To realize the mm-wave SEFDM experiment, both software and hardware are developed. The hardware testbed including analogue signal generation, integrated RoF and mm-wave wireless link and analogue signal reception will be described in section III. This section focuses on the software testbed. The software consists of two digital signal processing (DSP) blocks for digital signal generation and digital signal reception, at the transmitter and the receiver, respectively. The DSP modules of the mm-wave SEFDM transmission system are depicted in Fig. 2.

In line with most of today's wireless systems, forward error correction (FEC), in the form of convolutional coding, is applied in this system to achieve coding gain. A simple, rate 1/2 recursive systematic convolutional (RSC) code [24] is used, which is similar to the code used in FTN [17] and wireless based SEFDM [12]. At the transmitter, the input binary bits are first encoded in the RSC encoder. Then, a random interleaver Π is employed to permute the coded bits. Depending on the specific modulation format, the interleaved bits are mapped to the corresponding complex symbols. One uncoded pilot symbol is inserted at the beginning of each data stream and is used to estimate channel state information (CSI), enabling compensation for wireless channel distortion, imperfect timing synchronization and sampling phase offset. After the serial-to-parallel (S/P) conversion, oversampling is operated by adding zeros (i.e. guard band). The data stream with pilot symbols is modulated using a purpose designed SEFDM IFFT block [25]. Then a cyclic prefix (CP) is added at the beginning of each modulated symbol to combat multipath delay spread. In order to estimate the actual starting point of a data stream at the receiver, the Schmidl and Cox timing synchronization sequence [26] is added after the parallel-to-serial (P/S) conversion module.

In a direct detection optical system, to avoid the second-order intermodulation distortion (IMD) from the photo-detector (PD), a frequency gap [27] is introduced between the signal band and the optical carrier and is set to be at least equal to the bandwidth of the signal. This is typically done in the analogue domain using an IQ mixer which up converts baseband I and Q signals to a real value signal at a radio frequency f_c. In this work, in order to simplify the optical testbed, the IQ mixer function is realized in the DSP testbed. After adding the timing sequence, a serial data stream is upsampled to 12 GHz (i.e. arbitrary waveform generator (AWG) sampling frequency). Subsequently, the I and Q data of the upsampled SEFDM signal are up converted to f_c=1.8 GHz as:

$$x_{up}(m) = \Re\{x(m)\}cos(2\pi f_c m) + \Im\{x(m)\}sin(2\pi f_c m) \tag{1}$$

where $\Re\{\cdot\}$ and $\Im\{\cdot\}$ indicate the real and imaginary part of a signal, m is the time sample index and $x(m)$ is the upsampled baseband SEFDM signal at the transmitter. Then the mixed real valued SEFDM signal $x_{up}(m)$ is uploaded in a digital form to the AWG which implements a digital to analogue conversion. Finally, the AWG analogue output signal is transmitted through the fiber/wireless environment. It should be noted that all the signal processing within the transmitter DSP block is operated offline in a Matlab environment.

At the receiver, a real-time oscilloscope captures the analogue signal and transforms it to digital samples, with a 50 GHz sampling frequency, to be delivered to the receiver DSP block for offline processing. The down conversion and down
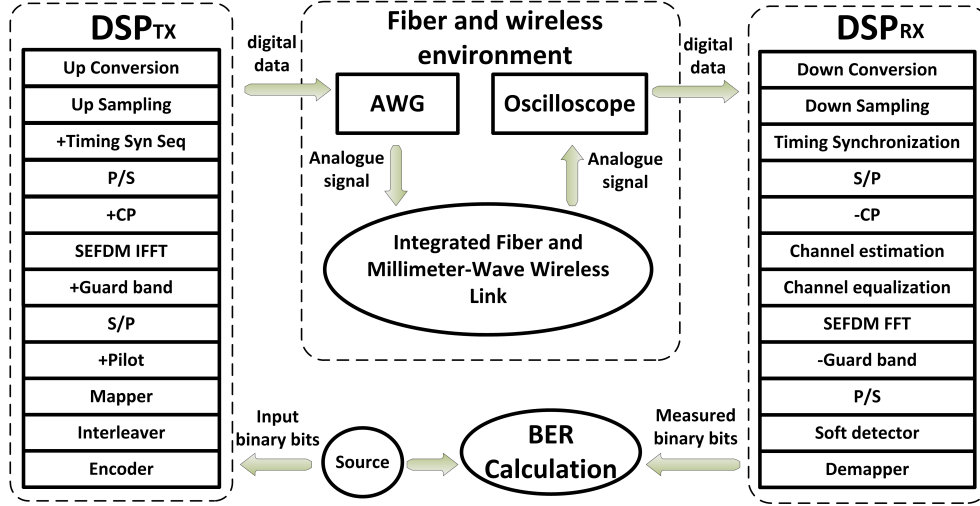
Figure 2. Block diagram of step-by-step digital signal processing operations for the mm-wave SEFDM transmission system.

sampling functions are realized in the receiver DSP block. The down conversion effectively implements the operation below

$$y_{down}(m) = y(m) \cdot e^{j2\pi f_c m} \qquad (2)$$

where m is the receiver sample index which has a larger sample range due to unbalanced sampling frequencies of the oscilloscope (i.e. 50 GHz) and the AWG (i.e. 12 GHz). It should be noted that $y(m)$ is the real valued sample from the oscilloscope while $y_{down}(m)$ is a complex signal, which includes I and Q data. After the down conversion and down sampling, the accurate starting point of the data stream is estimated according to the Schmidl and Cox algorithm [26]. In the mm-wave radio environment, the channel introduces amplitude attenuation, phase distortion and propagation delay. Additionally, imperfect timing synchronization leads to an inaccurate estimate of the starting point of a data stream. A small time offset results in the rotation of the constellation and degrades system performance, which, for design purposes, may be considered as an additional channel imperfection that can be corrected using channel equalization. For the purpose of channel compensation, a parallel signal is obtained after the S/P block and the CP is stripped away. Then, a channel estimation algorithm is employed to extract the CSI which is further used to equalize the distorted symbols. The compensated signal is demodulated using either the single FFT or the multiple FFTs methods [25]. After the removal of guard band and P/S conversion, the soft detector [28] is needed to recover SEFDM symbols from interference. Then, the recovered complex symbols are demapped to binary bits. Finally, the measured binary bits are compared with the original input binary bits for the BER calculation. The description above also applies to OFDM signal transmission.

A. Signal Model

Using the same number of sub-carriers N, SEFDM can save $(1 - \alpha) \times 100\%$ of bandwidth compared to OFDM. The bandwidth compression factor $\alpha = \Delta f T$ where Δf is the sub-carrier spacing and T is the period of one SEFDM symbol.

The mathematical expression of the SEFDM signal is shown in (3) as

$$X[k] = \frac{1}{\sqrt{Q}} \sum_{n=0}^{N-1} s_n e^{\frac{j2\pi n k \alpha}{Q}} \qquad (3)$$

where $X[k]$ is the kth time sample with $k = [0, 1, ..., Q-1]$, $Q = \rho N$ and $\rho \geq 1$ is the oversampling factor, $\frac{1}{\sqrt{Q}}$ is a normalization scaling factor and s_n is a QAM symbol modulated on the nth sub-carrier.

To simplify presentation and for ease of mathematical manipulation, matrix form is used as

$$X = \mathbf{F}S \qquad (4)$$

where X is a Q-dimensional vector of time samples of the transmitted signal, S is an N-dimensional vector of the QAM data symbols and $\mathbf{F}$ is a $Q \times N$ sub-carrier matrix with elements equal to the SEFDM complex sub-carriers $e^{\frac{j2\pi n k \alpha}{Q}}$.

B. Signal Generation and Detection

In a conventional OFDM system (i.e. α=1), the signal in (3) can be efficiently generated using inverse fast Fourier transform (IFFT). However, for an SEFDM signal (i.e. $\alpha < 1$), the IFFT approach is not straightforward. Two alternative methods were proposed in [25] where a single IFFT or multiple IFFTs can be applied for SEFDM.

A variety of detectors have been proposed to recover SEFDM signals from inter carrier interference (ICI) [29]. Among these, an iterative detection scheme is highly efficient due to its feedforward and feedback architecture. Turbo-SEFDM [28] follows the same idea that maximizes the *a posteriori* probability (APP) for a given bit through a process of iteration. This technique was conceptually described in [28] and later experimentally evaluated in [12][13][14].

C. Channel Compensation

Channel compensation can effectively deal with multipath fading, imperfect timing synchronization and sampling phase

offset issues. A single tap frequency-domain channel compensation algorithm is applied in an OFDM system while this is not possible for an SEFDM system due to the loss of orthogonality. Therefore, a time-domain channel compensation scheme is briefly described in this section and will be used in the experiment. The receiver signal model is expressed as

$$Y_{CP} = \mathbf{H}X_{CP} + Z_{CP} \tag{5}$$

where X_{CP} is the transmitted signal including both useful data and CP where the CP length is N_{CP}. $\mathbf{H}$ is a $U \times U$ channel matrix, where $U = Q + N_{CP}$ and Z_{CP} is the AWGN vector of length U. After CP removal, we obtain

$$Y_c = \mathbf{H_c}X + Z = \mathbf{H_c}\mathbf{F}S + Z \tag{6}$$

where Y_c, X and Z are the sample vectors after removing the first N_{CP} samples of Y_{CP}, X_{CP} and Z_{CP}, respectively. $\mathbf{H_c}$ is a $Q \times Q$ circulant matrix. A known pilot SEFDM symbol P is transmitted prior to user data signals. Thus, at the receiver the pilot signal is expressed as

$$Y_{c-pilot} = \mathbf{H_c}X + Z = \mathbf{H_c}\mathbf{F}P + Z \tag{7}$$

The first step is to estimate the channel matrix $\mathbf{H_c}$. Due to the circulant characteristic of $\mathbf{H_c}$, its first column gives all the information needed to reconstruct the matrix. By rearranging (7), a new expression is derived as

$$Y_{c-pilot} = \mathbf{P}h + Z \tag{8}$$

where h is a $Q \times 1$ vector and $\mathbf{P}$ is a $Q \times Q$ circulant matrix whose first column is equal to the vector $X = \mathbf{F}P$. Then $\hat{h}$, which is the estimate of h, is expressed as

$$\hat{h} = \mathbf{P}^*(\mathbf{PP}^*)^{-1}Y_{c-pilot} \tag{9}$$

where $\hat{h}$ is used to reconstruct the matrix $\mathbf{H_c}$ via copying and shifting $\hat{h}$ repeatedly.

The second step is to equalize the distorted SEFDM symbols in (6) using $\hat{\mathbf{H}}_\mathbf{c}^{-1}$, which is the inverse of the estimated channel matrix $\mathbf{H_c}$. Thus, compensated time samples are obtained for the following signal demodulation and detection stages.

III. EXPERIMENTAL SETUP

In this section, the mm-wave SEFDM signal transmission is experimentally tested in an indoor propagation environment using the testbed shown in Fig. 3, with the parameters shown in Table I. The 4QAM modulated SEFDM/OFDM signals of 1.125 GHz bandwidth, with different bit rates; specifically 2.25 Gbit/s for OFDM, 2.8 Gbit/s for α=0.8 and 3.75 Gbit/s for α=0.6 are generated offline in the DSP-Tx module in Fig. 2. Data streams are generated by assembling up to 10^6 coded bits per stream (over 6,250 OFDM/SEFDM symbols), with three additional uncoded symbols inserted at the start of an entire data stream; two symbols for timing synchronization and one symbol for channel estimation. BER measurements were taken for each transmitted stream and repeated several times for verification of measurement accuracy. Data stream samples are then uploaded to a Tektronix 7122B AWG operating at a sampling rate of 12 GS/s. After a 20 dB gain amplifier and a band-pass filter, the resulting signals are modulated onto

an optical carrier using a distributed feedback (DFB) laser at around 1554 nm and an intensity modulator biased at quadrature point. This results in an optical double sideband (DSB) signal at the output of a 3 GHz bandwidth Mach-Zehnder modulator (MZM). The optical signal is then transmitted over a 250 meters OM-1 MMF span, coupled using single mode fiber (SMF) connectors at both ends. An SMF-MMF(OM-1)-SMF link [30] is preferred to achieve a restricted mode launch condition, thus improving the bandwidth length product of graded index (GI)-MMFs, which is in the order of 500/160 MHz.km at 1310/850 nm, when operating in an overfilled launch condition (OFL). In the authors' recent work [16], a description of a purely optical system (that does not include the 60 GHz mm-wave link) is included as a first step towards the design of the 60 GHz system which is briefly described in the same reference.

Table I
EXPERIMENTAL SYSTEM SPECIFICATIONS

Parameters	Values
Millimeter wave frequency	60 GHz
Intermediate frequency	1.8 GHz
Baseband signal sampling frequency	3 GHz
Bandwidth of baseband signal	1.125 GHz
AWG sampling frequency	12 GHz
Oscilloscope sampling frequency	50 GHz
Length of MMF fiber	250 meters
Distance of mm-wave wireless link	3 meters
Modulation scheme	4QAM
IFFT/FFT size	128
Data sub-carriers	48; 60; 72; 80
Sub-carrier baseband bandwidth	23.4 MHz
Sub-carrier spacing	$\alpha \times 23.4$ MHz
Cyclic prefix	10
Channel coding	(7,5) RSC code
Coding rate	R_{code}=1/2

At the BS, a second uncorrelated DFB laser, tuned to 60 GHz below the optical frequency of the first DFB laser is combined in the 3 dB coupler with the DSB optical signal. The combined signal is attenuated using a variable optical attenuator (VOA) and delivered to a 70 GHz bandwidth photodiode. It is well-known that the phase noise of the optical carrier generated by the beating of two uncorrelated optical sources, as it is the case for the remote heterodyne detection scheme used in this experiment, may manifest itself in the broadening of the spectral linewidth. Also, in the presence of phase noise, a carrier-recovery circuit might have difficulties in tracking rapid phase variations, resulting in degradation of the detection performance. Alternatively, these phase-noise effects can be avoided at baseband by utilizing an envelope detector with sufficient IF bandwidth [31]. The measured optical spectrum at the VOA input is shown in Fig. 4 (a) where two wavelengths are shown with a 60 GHz separation. The detailed DSB signal spectrum is also illustrated in the inset of the same figure. The 60 GHz mm-wave signal can be generated at the 70 GHz square-law photodiode based on an uncorrelated remote heterodyne detection (RHD) scheme. This optical scheme is of low-cost and can be easily used for existing 4G or future 5G mm-wave signal by adjusting the
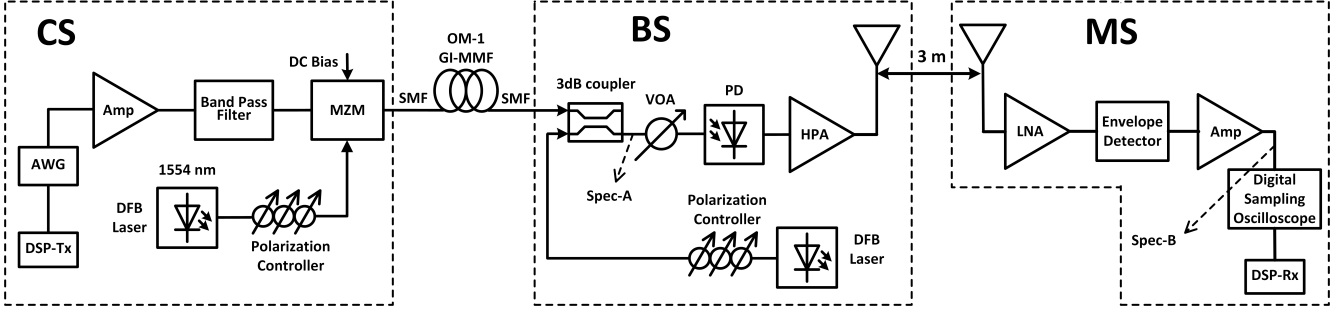
Figure 3. Experimental setup for SEFDM signal transmission over a 60 GHz millimeter-wave radio over fiber transmission link.
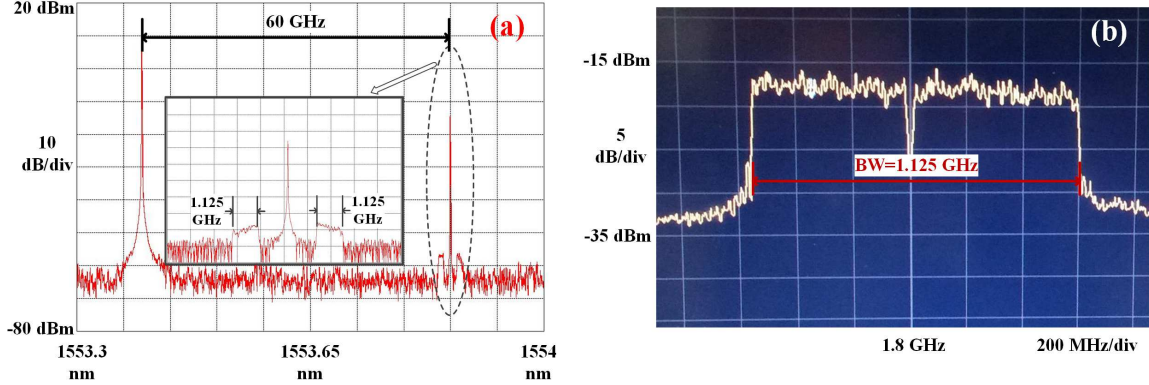

Figure 4. Optical and electrical spectra illustration. (a) Spec-A in Fig.3. (b) Spec-B in Fig. 3.

laser separation to any required carrier frequencies.

A pair of 60 GHz parabolic (Cassegrain) antennas operating in the frequency range of 50-75 GHz which have 30 dBi gain; and 3 dB beamwidth of 3.1° are employed. In addition, a 30 dB gain V-band high power amplifier (HPA) at the transmitter and a 30 dB gain V-band low noise amplifier (LNA) at the receiver are used. Having propagated through a 3 meter mm-wave wireless link, the received 60 GHz mm-wave signal is down-converted to a 1.8 GHz intermediate frequency (IF) using a waveguide coupled 3 GHz bandwidth envelope detector, which is tolerant of phase noise impairment. The IF signal is captured by a real-time digital oscilloscope and the measured electrical spectrum is illustrated in Fig. 4 (b) where the signal bandwidth is 1.125 GHz. Finally, the captured signal is processed offline in the DSP-Rx module as detailed in Fig. 2.

The system parameters used in this experiment are given in Table I. In this experiment, a total of 1.125 GHz data bandwidth is used. The number of data sub-carriers is different for the OFDM and SEFDM systems. For OFDM, 48 data sub-carriers are used while with higher bandwidth compression levels in SEFDM systems, more data sub-carriers (e.g. 60 for α=0.8, 72 for α=0.67 and 80 for α=0.6) are aggregated.

IV. RESULTS AND DISCUSSION

As mentioned before, in order to simplify the optical testbed, up sampling and up conversion to IF are moved to the digital domain and performed by the DSP elements in Fig. 2.
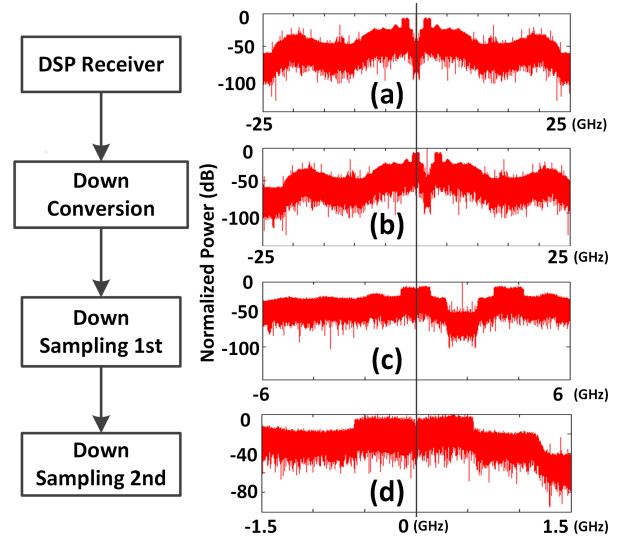

Figure 5. Signal spectra at different receiver stages.

Electrical spectra at different receiver stages are shown by the insets in Fig. 5. For the illustration, only OFDM spectra are shown here. First, the received spectrum from the 50 GS/s real-time oscilloscope is shown in Fig. 5 (a). The overall frequency range is 50 GHz indicating the sampling frequency of the oscilloscope. Two peaks are observed indicating double sideband signal with 1.125 GHz bandwidth for each one. After

down conversion, one side band is moved to baseband as shown in Fig. 5 (b). Due to the unbalanced sampling frequency (12 GHz AWG and 50 GHz oscilloscope), two-stage down sampling is required. The first stage is from 50 GHz to 12 GHz in Fig. 5 (c) and the second one is from 12 GHz to 3 GHz in Fig. 5 (d). Then the baseband signal is timing synchronized for subsequent signal processing.

Measured receiver constellation diagrams for OFDM and SEFDM (i.e. α=0.8) signals are illustrated in Fig. 6 in the form of constellation density plots. Two channel compensation scenarios are considered to recover the rotated constellation points. For the OFDM signal, a typical frequency-domain channel compensation algorithm is employed. For the SEFDM signal, an additional time-domain channel compensation scheme is also tested. The purpose of the comparison is to show the effects of two channel compensation schemes on the SEFDM signal.
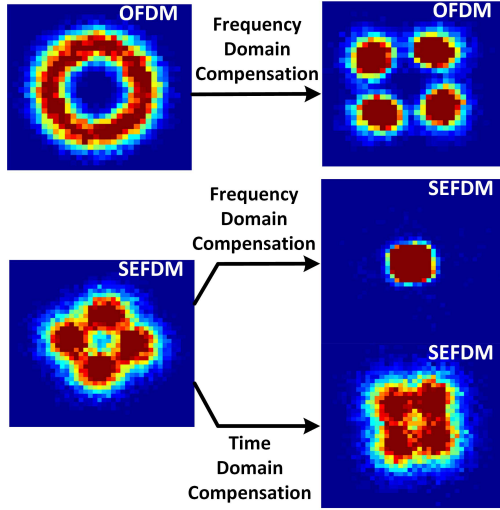

Figure 6. Constellation diagrams for OFDM and SEFDM (i.e. α=0.8) signals before and after channel compensation.

It is evident that due to sampling phase offset and imperfect timing synchronization, both the original OFDM and SEFDM signal constellation points are scattered and overlapped. For OFDM, before channel compensation, the constellation points rotate in phase and appear as a circle. After applying frequency-domain channel compensation, the phase rotation can be mitigated and the constellation points are clearly distinguishable. However, for the SEFDM signal, following the same frequency-domain channel compensation, the phase ambiguity is not mitigated. The constellations are no longer recoverable. This is because the non-orthogonality between sub-carriers results in compensation failure. The constellation recovery can be achieved using the aforementioned time-domain channel compensation. Hence, the recovered constellation is recognized. It should be noted that compared to the recovered OFDM, the SEFDM with time-domain channel compensation shows more scattered constellation points due to the self-created ICI of SEFDM signals. The intrinsic ICI will be mitigated using the soft signal detection mechanism [28].
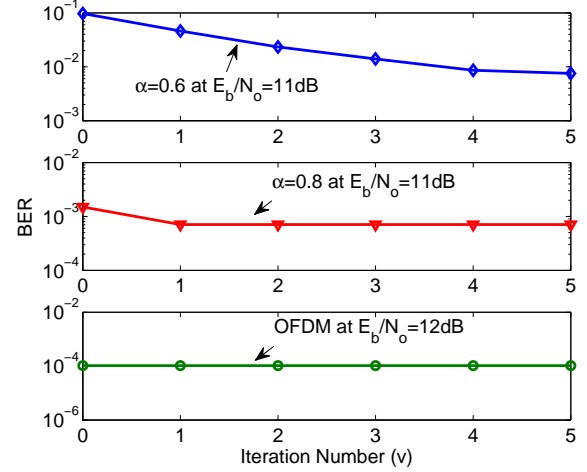

Figure 7. BER convergence performance of SEFDM signals over the integrated 60 GHz mm-wave and fiber transmission link.

The iteration performance is evaluated in Fig. 7 in terms of the number of iterations (v). It is evident that no iteration is needed for the OFDM system. However, for SEFDM systems, in order to get converged performance, extra iterations are required to deal with the interference introduced by the closer packing of sub-carriers. Thus, SEFDM requires additional computations to get converged performance. For α=0.8, one iteration is sufficient while four iterations are needed for α=0.6. This is due to the fact that with smaller α (i.e. higher bandwidth compression), more ICI is introduced. The computational complexity for SEFDM is flexible based on variable implementation methods such as pruned and non-pruned FFT operations. The detailed analysis of complexity can be found in [25][28].

BER performance was measured and shown in Fig. 8. Two typically used FEC limits [32] are indicated in the figure to facilitate comparison of power penalties when SEFDM is used. It is clearly seen that by using α=0.8, the BER performance is close to that of the 4QAM modulated OFDM system. This proves that occupying the same bandwidth, the SEFDM system can transmit more data. For the SEFDM system with a higher level of bandwidth compression such as α=0.6 and therefore higher interference, the performance is degraded with an approximately 3 dB power penalty relative to OFDM, at all values measured for BER below 2×10^{-2} as shown in the figure. In addition, two systems with equal spectral efficiencies operating in the same bandwidth are evaluated. The first is an OFDM system with 8QAM modulated symbols and the second is a 4QAM SEFDM system of α=0.67. The results, also plotted in Fig. 8, clearly show that the α=0.67 SEFDM outperforms OFDM of equal spectral efficiency with 1 dB gain. It is also worth noting that the case of α=0.6 also outperforms the 8QAM OFDM in both spectral efficiency and BER performance. In other words, the above indicates that a lower order modulation format, with the advantage of increased bit rate, can replace a higher order one without compromising BER performance.

as

$$R_d = \frac{1}{\alpha} \times (1 - BER) \times B \times log_2 O \qquad (10)$$

where B is data bandwidth, BER is the bit error rate at a specific E_b/N_o value, $(1 - BER)$ indicates the probability of a non-error received bit stream and O is the constellation cardinality. For the 4QAM cases studied, Table II shows the SEFDM benefits in terms of spectral efficiencies and achievable bit rates, for different bandwidth compression factors and associated number of sub-carriers. Although SEFDM shows slight performance degradation, it is apparent in Fig. 9 that the gross bit rates of 4QAM SEFDM with different bandwidth compression factors are higher than that of 4QAM OFDM. This is because compared to OFDM, in the SEFDM scenario, more sub-carriers are packed into a given bandwidth with a much closer sub-carrier spacing. For higher order modulation formats such as 8QAM, a spectral efficiency equivalent 4QAM shows a higher bit rate due to the 1 dB performance gain achieved in Fig. 8.
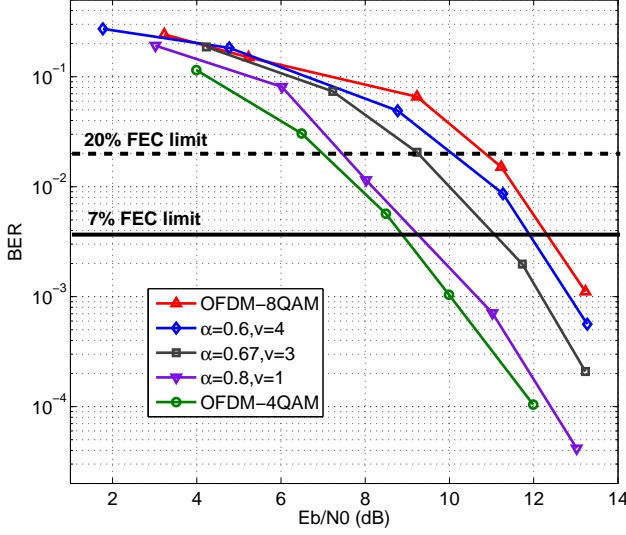

Figure 8. BER performance of SEFDM signals at 60 GHz mm-wave frequency through 3 meters wireless and 250 meters MMF fiber transmission with 4QAM symbols.
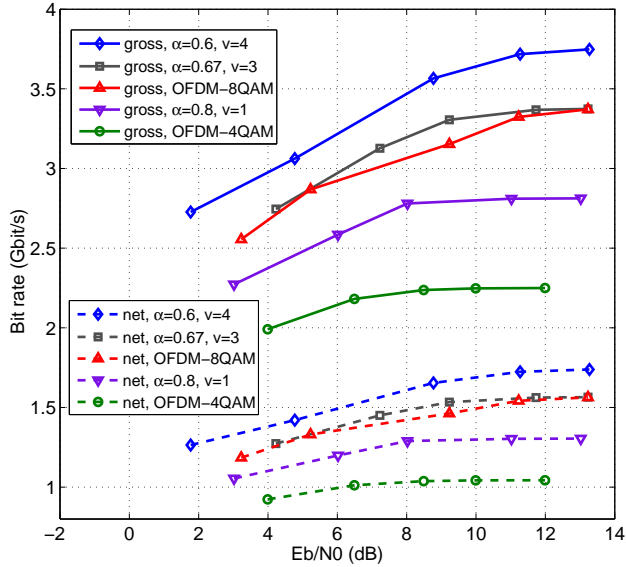
Table II
GROSS SPECTRAL EFFICIENCY AND BIT RATE COMPARISONS
(4QAM-1.125 GHz BANDWIDTH)

Parameter	OFDM	SEFDM		
α	1	0.8	0.67	0.6
Data sub-carriers	48	60	72	80
Spectral efficiency (bit/s/Hz)	2.0	2.5	3.0	3.3
Bit rate (Gbit/s)	2.25	2.80	3.38	3.75

In addition, net bit rates are also illustrated in Fig. 9 for SEFDM and OFDM after removing the CP and coding redundancy bits. We note that the pilot symbol and the timing sequence are used only once at the beginning of a data stream and therefore have minimal contribution to the size of the overhead and a negligible effect on the calculation of net bit rate.

V. CONCLUSIONS

This work introduces a new framework to improve data rates, in a millimeter-wave RoF system, within a limited bandwidth and without changing the transmission rate per sub-carrier, by using bandwidth compressed spectrally efficient FDM (SEFDM) signals. Experimental results demonstrate the efficacy of SEFDM through showing that the bit rate can be increased whilst maintaining the same bandwidth, at the expense of some power penalty. For a 4QAM OFDM system, occupying 1.125 GHz bandwidth, the gross bit rate can reach 2.25 Gbit/s at E_b/N_o=12 dB, while, for similar E_b/N_o values in an SEFDM system, compressing the sub-carrier spacing by 20%, it can achieve 2.8 Gbit/s. With further bandwidth compression of 40%, results show that up to 3.75 Gbit/s can be achieved at the expense of a loss (around 3 dB) in error performance and additional computational complexity. In addition, the two spectral efficiency equivalent systems 4QAM SEFDM and 8QAM OFDM are experimentally demonstrated. The SEFDM system is shown to outperform the 8QAM OFDM with 1 dB performance gain. All experimental results were obtained by testing signals over a wireless channel using a pair of antennas operating in the 60 GHz mm-wave band.

Figure 9. Gross and net bit rates of SEFDM signals at 60 GHz mm-wave through 3 meters wireless and 250 meters MMF fiber transmission with 4QAM symbols.

Due to unreliable transmission links, errors are introduced. Therefore, the effective bit rate, which is related to BER values, is smaller than the theoretical one. The effective gross bit rate is defined as the non-error bits per second that can be achieved including overhead (i.e. symbols used for channel estimation, syncronization), CP and coding redundancy bits. Effective gross bit rates are plotted for three different systems at different E_b/N_o values in Fig. 9 following the calculation

References

[1] 3GPP TR 36.912 v.13.0.0, "Feasibility study for further advancements for E-UTRA (LTE-Advanced)," Rel. 13, Dec. 2015.

[2] T. S. Rappaport, S. Sun, R. Mayzus, H. Zhao, Y. Azar, K. Wang, G. N. Wong, J. K. Schulz, M. Samimi, and F. Gutierrez, "Millimeter wave mobile communications for 5G cellular: It will work!" *IEEE Access*, vol. 1, pp. 335–349, May 2013.

[3] V. Thomas, M. El-Hajjar, and L. Hanzo, "Performance improvement and cost reduction techniques for radio over fiber communications," *Communications Surveys Tutorials, IEEE*, vol. 17, no. 2, pp. 627–670, Second quarter 2015.

[4] J. Andrews, S. Buzzi, W. Choi, S. Hanly, A. Lozano, A. Soong, and J. Zhang, "What will 5G be?" *Selected Areas in Communications, IEEE Journal on*, vol. 32, no. 6, pp. 1065–1082, June 2014.

[5] L. L. Hanzo, M. Münster, B. J. Choi, and T. Keller, *OFDM and MC-CDMA for broadband multi-user communications, WLANs and broadcasting*. Wiley-IEEE Press, 2003.

[6] E. P. Martin, T. Shao, V. Vujicic, P. M. Anandarajah, C. Browning, R. Llorente, and L. P. Barry, "25-Gb/s OFDM 60-GHz radio over fiber system based on a gain switched laser," *Journal of Lightwave Technology*, vol. 33, no. 8, pp. 1635–1643, April 2015.

[7] M. Weiss, A. Stohr, F. Lecoche, and B. Charbonnier, "27 Gbit/s photonic wireless 60 GHz transmission system using 16-QAM OFDM," in *Microwave Photonics, 2009. MWP '09. International Topical Meeting on*, Oct 2009, pp. 1–3.

[8] A. Kanno, K. Inagaki, I. Morohashi, T. Sakamoto, T. Kuri, I. Hosako, T. Kawanishi, Y. Yoshida, and K. i. Kitayama, "40 Gb/s W-band (75-110 GHz) 16-QAM radio-over-fiber signal generation and its wireless transmission," in *Optical Communication (ECOC), 2011 37th European Conference and Exhibition on*, Sept 2011, pp. 1–3.

[9] M. Rodrigues and I. Darwazeh, "A spectrally efficient frequency division multiplexing based communications system," in *Proc. 8th Int. OFDM Workshop*, Hamburg, 2003, pp. 48–49.

[10] D. Rainnie, Y. Feng, and J. Bajcsy, "On capacity merits of spectrally efficient FDM," in *Military Communications Conference, MILCOM 2015 - 2015 IEEE*, Oct 2015, pp. 581–586.

[11] I. Kanaras, A. Chorti, M. Rodrigues, and I. Darwazeh, "Spectrally efficient FDM signals: Bandwidth gain at the expense of receiver complexity," in *Communications, 2009. ICC '09. IEEE International Conference on*, June 2009, pp. 1–6.

[12] T. Xu and I. Darwazeh, "Bandwidth compressed carrier aggregation," in *IEEE ICC 2015 - Workshop on 5G & Beyond - Enabling Technologies and Applications (ICC'15 - Workshops 23)*, London, United Kingdom, Jun. 2015, pp. 1107–1112.

[13] I. Darwazeh, T. Xu, T. Gui, Y. Bao, and Z. Li, "Optical SEFDM system; bandwidth saving using non-orthogonal sub-carriers," *Photonics Technology Letters, IEEE*, vol. 26, no. 4, pp. 352–355, Feb 2014.

[14] D. Nopchinda, T. Xu, R. Maher, B. Thomsen, and I. Darwazeh, "Dual polarization coherent optical spectrally efficient frequency division multiplexing," *Photonics Technology Letters, IEEE*, vol. 28, no. 1, pp. 83–86, Jan 2016.

[15] S. Mikroulis, T. Xu, J. Mitchell, and I. Darwazeh, "First demonstration of a spectrally efficient FDM radio over fiber system topology for beyond 4G cellular networking," in *Networks and Optical Communications - (NOC), 2015 20th European Conference on*, June 2015, pp. 1–5.

[16] S. Mikroulis, T. Xu, and I. Darwazeh, "Practical demonstration of spectrally efficient FDM millimeter-wave radio over fiber systems for 5G cellular networking," in *Proc. SPIE*, vol. 9772, 2016, pp. 97 720I–1–97 720I–8.

[17] J. Anderson, F. Rusek, and V. Öwall, "Faster-than-Nyquist signaling," *Proceedings of the IEEE*, vol. 101, no. 8, pp. 1817–1830, 2013.

[18] A. Barbieri, D. Fertonani, and G. Colavolpe, "Time-frequency packing for linear modulations: spectral efficiency and practical detection schemes," *Communications, IEEE Transactions on*, vol. 57, no. 10, pp. 2951–2959, October 2009.

[19] M. Secondini, T. Foggi, F. Fresi, G. Meloni, F. Cavaliere, G. Colavolpe, E. Forestieri, L. Poti, R. Sabella, and G. Prati, "Optical time-frequency packing: Principles, design, implementation, and experimental demonstration," *Lightwave Technology, Journal of*, vol. 33, no. 17, pp. 3558–3570, Sept 2015.

[20] M. Rodrigues and I. Darwazeh, "Fast OFDM: a proposal for doubling the data rate of OFDM schemes," in *International conference on Telecommunications*, vol. 3, 2002, pp. 484–487.

[21] J. Zhao and A. D. Ellis, "A novel optical fast OFDM with reduced channel spacing equal to half of the symbol rate per carrier," in *Optical Fiber Communication (OFC), collocated National Fiber Optic Engineers Conference, 2010 Conference on (OFC/NFOEC)*, March 2010, pp. 1–3.

[22] H. Shams and J. Zhao, "First investigation of fast OFDM radio over fibre system at 60 GHz using direct laser modulation," in *Lasers and Electro-Optics Europe (CLEO EUROPE/IQEC), 2013 Conference on and International Quantum Electronics Conference*, May 2013.

[23] X. Ouyang, W. Jia, P. Gunning, P. D. Townsend, and J. Zhao, "Experimental demonstration and field-trial of an improved optical fast OFDM scheme using intensity-modulation and full-field detection," *Journal of Lightwave Technology*, vol. 33, no. 20, pp. 4353–4359, Oct 2015.

[24] C. Berrou and A. Glavieux, "Near optimum error correcting coding and decoding: turbo-codes," *IEEE Transactions on Communications*, vol. 44, no. 10, pp. 1261–1271, Oct 1996.

[25] P. Whatmough, M. Perrett, S. Isam, and I. Darwazeh, "VLSI architecture for a reconfigurable spectrally efficient FDM baseband transmitter," *Circuits and Systems I: Regular Papers, IEEE Transactions on*, vol. 59, no. 5, pp. 1107–1118, May 2012.

[26] T. Schmidl and D. Cox, "Robust frequency and timing synchronization for OFDM," *Communications, IEEE Transactions on*, vol. 45, no. 12, pp. 1613–1621, Dec 1997.

[27] B. Schmidt, A. Lowery, and J. Armstrong, "Experimental demonstrations of electronic dispersion compensation for long-haul transmission using direct-detection optical OFDM," *Lightwave Technology, Journal of*, vol. 26, no. 1, pp. 196–203, 2008.

[28] T. Xu and I. Darwazeh, "A soft detector for spectrally efficient systems with non-orthogonal overlapped sub-carriers," *Communications Letters, IEEE*, vol. 18, no. 10, pp. 1847–1850, Oct 2014.

[29] S. Isam and I. Darwazeh, "Characterizing the intercarrier interference of non-orthogonal spectrally efficient FDM system," in *Communication Systems, Networks Digital Signal Processing (CSNDSP), 2012 8th International Symposium on*, July 2012, pp. 1–5.

[30] S. Mikroulis, M. P. Thakur, and J. E. Mitchell, "Evaluation of OOK and OFDM on an SMF-MMF-SMF link targeting a PON/60-GHz topology for beyond 4G," *IEEE Photonics Technology Letters*, vol. 28, no. 4, pp. 449–452, Feb 2016.

[31] O. Omomukuyo, M. Thakur, and J. Mitchell, "Simple 60-GHz MB-OFDM ultrawideband RoF system based on remote heterodyning," *Photonics Technology Letters, IEEE*, vol. 25, no. 3, pp. 268–271, Feb 2013.

[32] F. Chang, K. Onohara, and T. Mizuochi, "Forward error correction for 100 G transport networks," *IEEE Communications Magazine*, vol. 48, no. 3, pp. S48–S55, March 2010.